

Supporting Information for:

Synthesis of Highly Monodisperse Citrate-Stabilized Silver Nanoparticles of up to 200 nm: Kinetic Control and Catalytic Properties

Neus G. Bastús, Florind Merkoçi, Jordi Piella and Victor Puntès

- 1. The Effect of Tannic Acid in the Final Morphology of Ag NPs**
- 2. Kinetics of Reduction Reaction**
- 3. Formation Mechanism of Ag Nanoparticles**
- 4. Calculated Mie Spectra**
- 5. Ligand Exchange of Ag Nanoparticles**

1. The Effect of Tannic Acid (TA) in the Final Morphology of Ag NPs

The addition of small amounts of Tannic Acid (TA) narrows the size distribution, producing highly monodisperse Ag NPs of 10.1 ± 0.9 nm in diameter (**Fig. S1**). These results correlate with the absorption profile observed by UV-Vis spectroscopy, displaying a sharp and rather symmetric plasmon band placed at ~ 397 nm. When running the reaction in the absence of TA, a broad band peaking at ~ 420 nm was obtained together with an increase of the full width at half maximum (FWHM) of the spectra from 58 to 83 nm. This broadening and the notable band asymmetry of the spectrum is representative of the wide dispersity of Ag NP's, particularly the presence of elongated oval-shaped, polyhedrons and plate-like Ag NPs, with a low nanosphere yield, as previously reported by Lee and Meisel¹. Interestingly, this improve in size dispersity is also associated to very high reaction yields, obtaining that Ag precursor conversion to metallic Ag is much higher when using TA as a co-reducer.

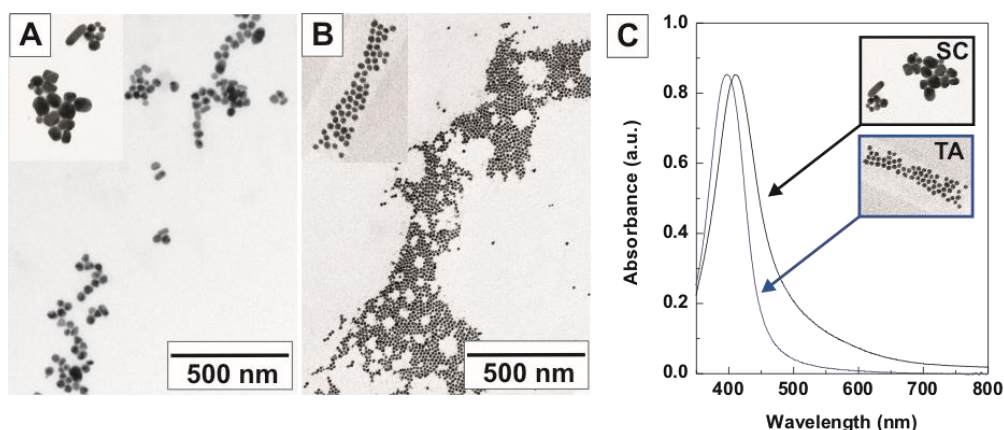


Figure S1- Effect of TA in the synthesis of citrate-stabilized Ag NPs. Transmission electron microscopy images and UV-Vis spectra of Ag NPs synthesized using sodium citrate (A, C-black spectrum) or a combination of SC and TA (B, C-blue spectrum).

Concentration of TA dictates the rate and extent of nucleation, with lower concentrations favoring fast nucleation and small particles, and larger (and less abundant) particles with higher size dispersity are produced as TA concentration increases. Similar results were reported by Dadosh in the synthesis of Ag NPs with diameters ranging from 18 to 30 nm² and by Rainville et al. in the synthesis of PVP-coated Ag NPs from 26 to 118 nm³. However, comparing these results with those obtained by Slot and Geuze for the synthesis of Au NPs⁴ the concentration of TA has the opposite effect, i.e., in the case of Au, increased concentrations of TA resulted in

smaller particles. This inverted dependence of Ag NP's size on TA concentration is related to its stronger ability to form complexes with Ag^+ ions as SC does. On the contrary, Au^{3+} , with a stronger oxidizer potential, do not form stable complexes with TA, therefore leading to the synthesis of smaller NPs (faster burst nucleation and higher number of Au NPs) when increasing TA concentration.

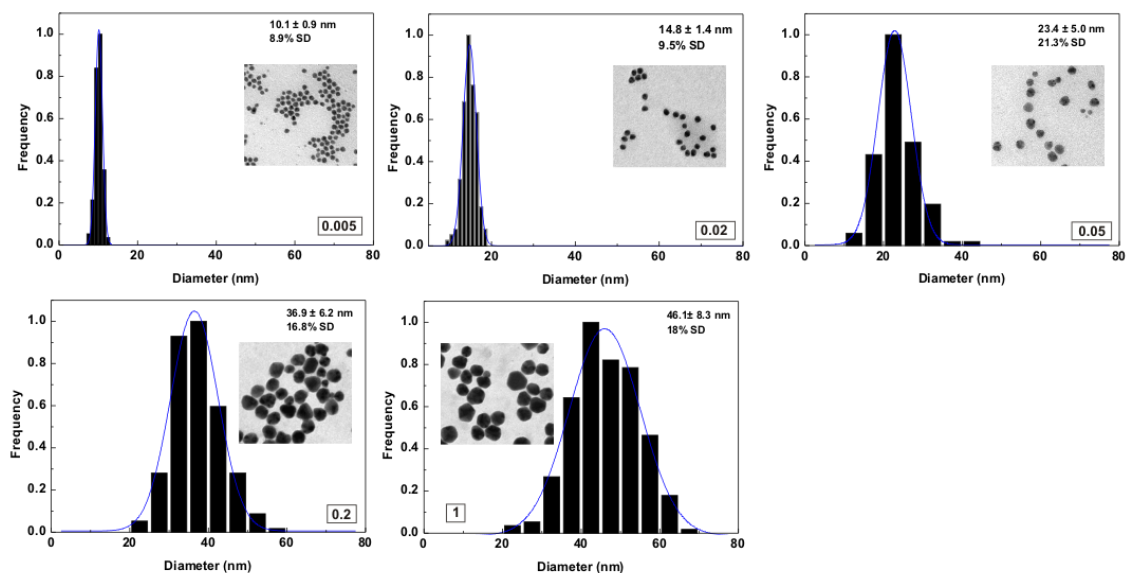


Figure S2- TEM image Analysis of Ag NPs shown in Figure 2A. Ag seed diameter increases from 10.1 ± 0.9 nm to 46.1 ± 8.3 nm by using different TA/SC ratios, from 0.005/1 to 1/1. At least, 500 NPs were counted in each case.

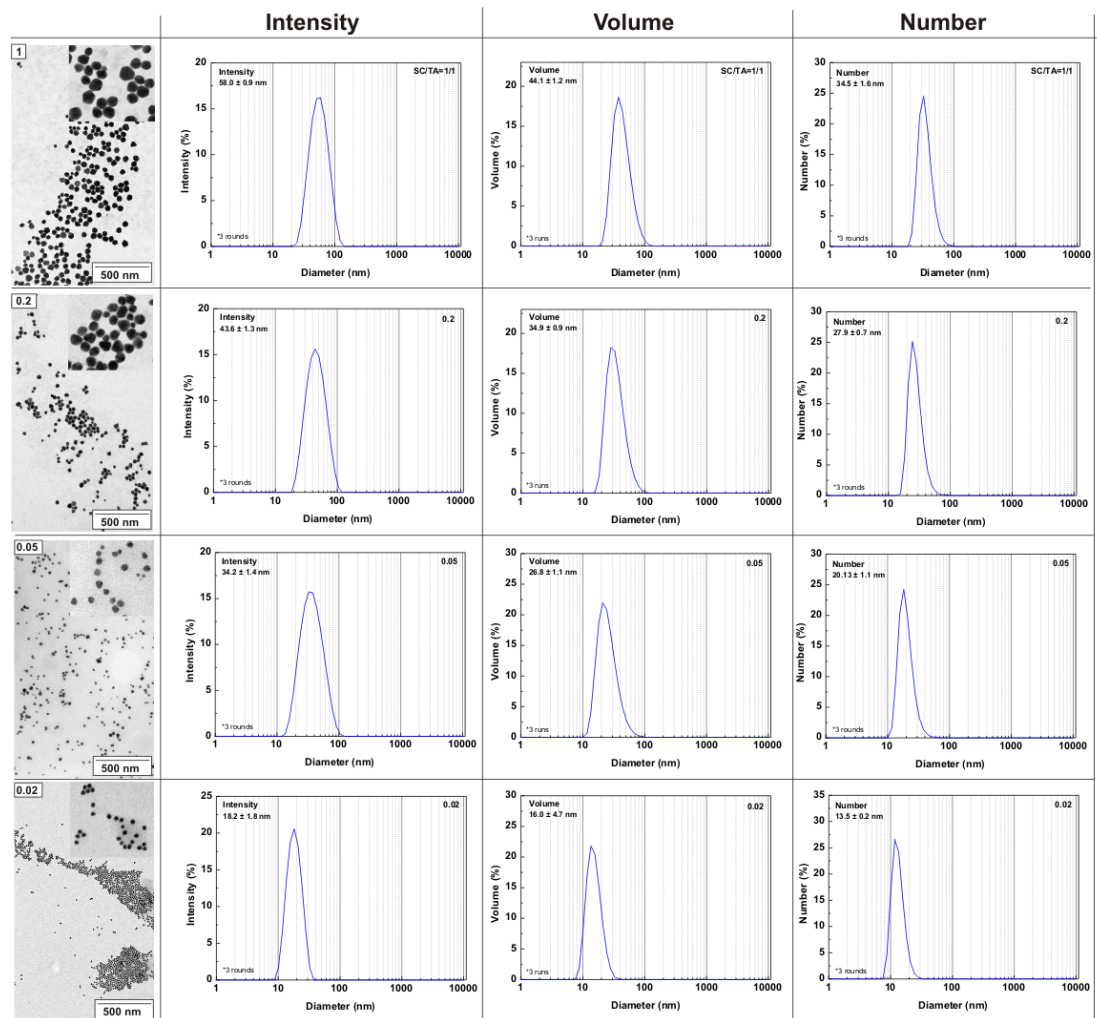
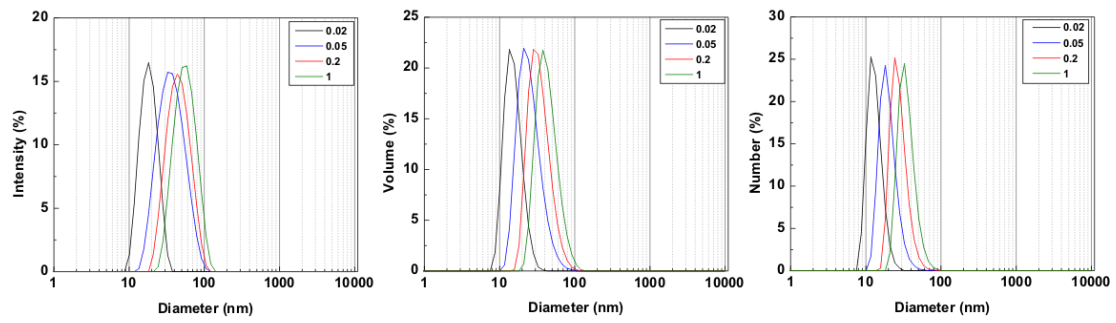


Figure S3- Size distribution measured by Dynamic Light Scattering. Size Distribution by Intensity, Volume and Number of Ag NPs synthesized by using different concentrations of TA.

2. Kinetics of Reduction Reaction

In order to understand the role of TA in the formation mechanism of Ag NPs, we studied the reduction reaction by monitoring the temporal evolution of UV-Vis spectra. Changes in the absorption spectra using a fixed concentration of TA (1 mM) are shown in **Figure S4-A,B**. As can be seen, at the initial stages of the reaction the solution presented a slightly yellow color which correlates with the appearance of a weak absorption band, initially peaking at ~418 nm. Then, as the reaction proceeded (1-10 min), the solution turned bright yellow and the absorption peak gradually blue-shifted from ~418 nm to ~410 nm. This continuous increase in the absorbance intensity was followed by a plateau state, where the absorbance remained almost unchanged.

Interestingly, time needed to reach the stationary state depends on the concentration of TA, being substantially faster in the low TA concentration regime (**Figure S4-C**). Thus, when the concentration of TA used was 0.1 mM the reaction took less than 10 min to reach the maximum absorbance value while it needed more than 30 min when TA concentration increased up to 1 mM. Similarly, the evolution of the SPR band and its final value also depend on the concentration of TA used, evolving slower and peaking at longer wavelengths (indicative of larger particles) for increasing concentration of TA (**Figure S4-D**). These results indicate that Ag NP's formation rate and final particle size is strongly determined by the concentration of TA used. Moreover, when comparing these results with those obtained in the direct citrate reduction (**Figure S4-C grey curve**) it can be seen how SC brings about slow growth of Ag NPs, needing more than 45 min to achieve a stationary growth stage. These results suggest the possibility to kinetically control the reduction of Ag ions by adding controlled amounts of TA to the reaction, which act as a primary reducer of the reaction, while SC plays the role of secondary reducer and stabilizer. Even more, a partial amount of TA can be used for nucleation while SC can drive the growth process once the catalytic nuclei are formed.

The dependence of Ag NP's morphology with the formation rate can be understood in terms of the commonly known La Mer model. Thus, a fast reduction leads to a burst nucleation, producing small nuclei which further grow to form, in homogeneous conditions, narrowly distributed NPs. On the contrary, if the reduction is slow, the nucleation overlaps with growth processes, easily leading to the inhomogeneous formation of particles, and consequently, in the difficulty of controlling their size

distribution. Although a fast reduction is typically associated with a strong reducing environment, we found herein the opposite behavior, i.e., the faster Ag NP's formation takes place at lower concentrations of TA, due to the strong complexing ability of TA stabilizing intermediate forms of Ag^+ ions⁵.

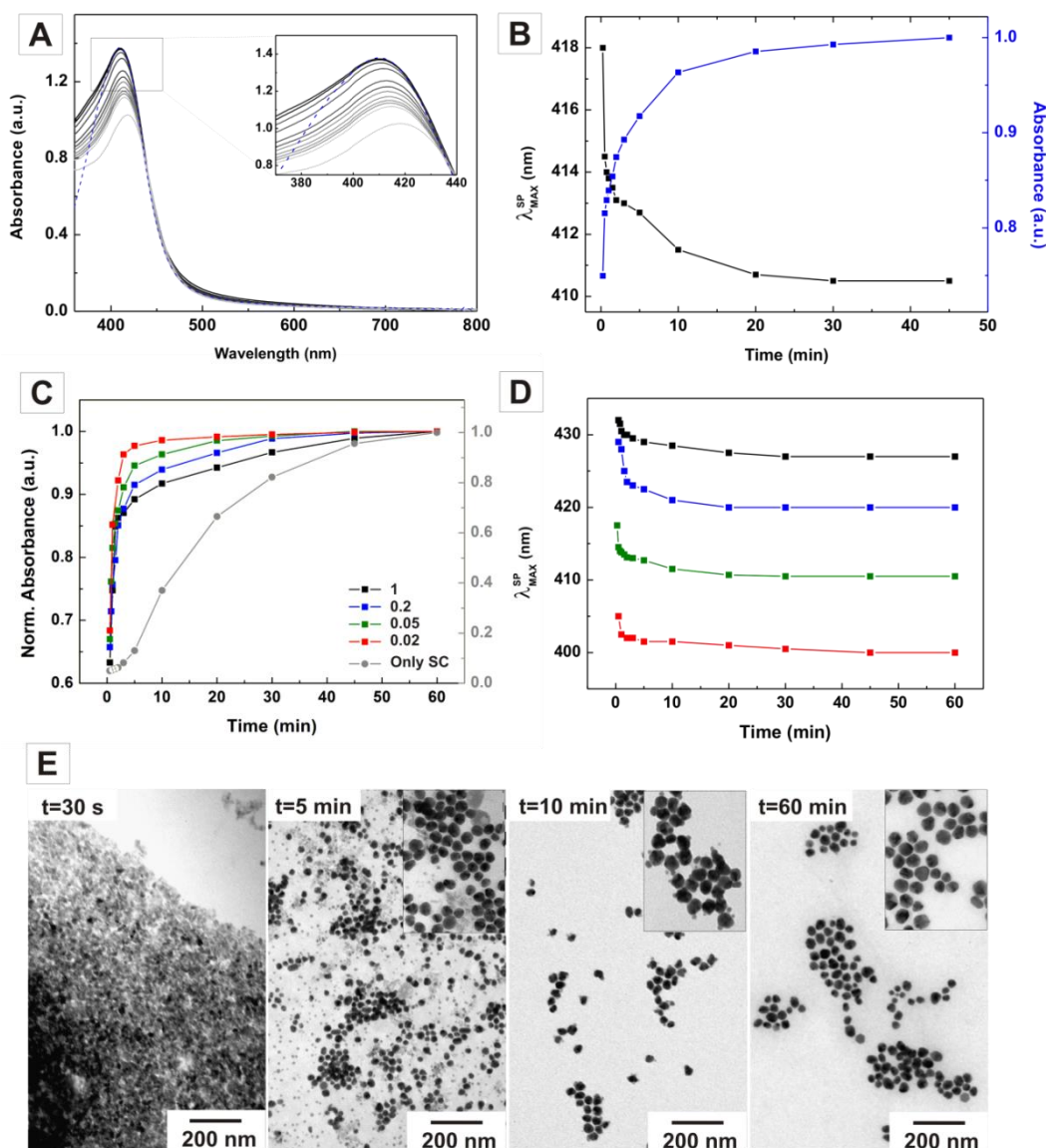


Figure S4- Kinetics of the Ag Reduction Reaction and Ag NP's Formation. (A) Time evolution UV-Vis spectra of Ag NPs obtained using 1mM of TA (TA/SC=0.02/1). Dotted-line corresponds to Ag NPs after the washing process. (B) Time evolution of the SPR band and the intensity maximum as a function of time for Ag NPs obtained using 1mM of TA (TA/SC=1/1). (C) Time evolution of the intensity maximum of Ag NP obtained using different concentrations TA, from 0.1mM (TA/SC=0.02/1) to 5mM (TA/SC=1/1). Results obtained using only SC were plot for comparison. (D) Time evolution of the SPR of Ag NP obtained using different concentrations TA, from 0.1mM to 5mM. (E) Representative TEM images of Ag NP grown at different times for TA/SC=0.2/1. The formation of inhomogeneous Ag

intermediates was observed at early stages (30 s) in which small particles formed (5 min) and then dissolved, acting as a source of atoms for the growth of large particles (10 min and 60 min).

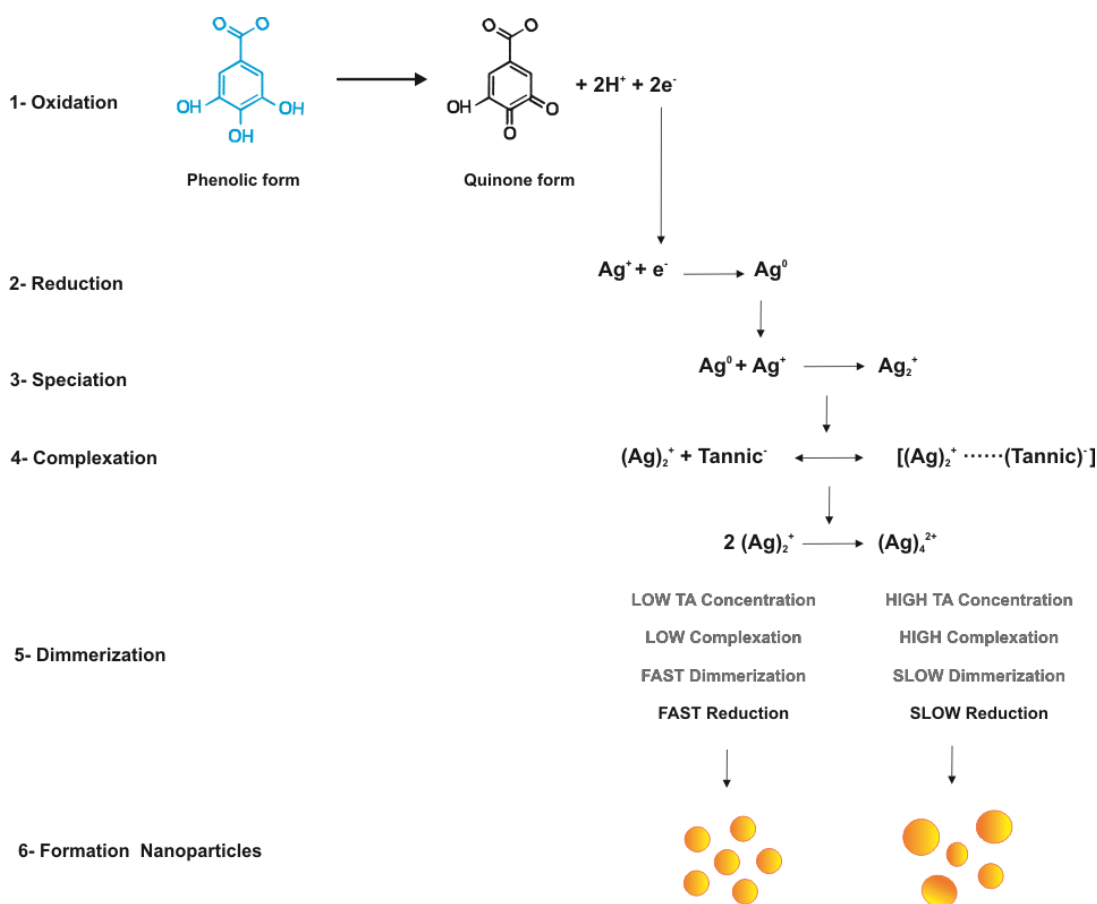
The study of the morphology at selected reaction times (and at a fixed concentration of TA, 1mM) provides further information. As can be seen in **Figure S4-D**, at short reactions times (30s), large and inhomogeneous fluffy intermediates were observed. As the reaction proceeded (5 min), the size of these intermediate products decreased while spherical, rather monodisperse Ag NPs appeared. These particles were accompanied by small-sized Ag NPs of 3-5 nm in diameter which progressively disappeared (10 min), acting as a temporal Ag reservoir and leading finally to well-defined Ag crystals. These results, together with the time-dependent evolution of the SPR band (**Figure S4-D**), suggest that nucleation of Ag NPs is mediated by the presence of small Ag aggregates, probably due to the complexation of Ag ions by TA formed at the early stages of the reaction. These intermediates species further dissolve acting as a source of atoms for the nucleation and growth of Ag NPs. Similar proto-particles in form of fluffy aggregates have also been observed at very short times in the citrate-mediated synthesis of Au NPs^{6,7}.

3. Formation Mechanism of Ag Nanoparticles

This formation process can be understood taking into account the interaction of silver precursor with TA, in particular the fact that a single reagent plays multiple roles, as reducing agent, stabilizer and complexation agent (**Scheme 1**). The representative structure of TA consists of a central core of glucose linked by ester bonds to polygalloyl ester chains, where phenolic hydroxyls undergo two-electron oxidation to the corresponding quinone form (**Scheme 1-1**) and donate two electrons for the reduction of Ag^+ precursor (**Scheme 1-2**). At this moment, a two-step process takes place, the production of Ag^0 and the further formation of a new species, Ag_2^+ ^{8,9} (**Scheme 1-3**). Later, the dimerization of Ag_2^+ leads to the formation of Ag_4^{2+} which acts as a monomer for the formation of Ag NPs. This reaction is influenced by the presence of TA, which readily interacts with Ag_2^+ , mediating its complexation with positively charged silver dimers at high concentrations (**Scheme 1-4**). This $[\text{Ag}_2^+\text{-TA}]$ complex undergoes slower transformations compared to the un-complexed Ag_2^+ , which leads to the formation of Ag NPs with irregular sizes. Obviously, this complexation depends on

the concentration of TA used, achieving higher complexation rates as the concentration of TA increases (**Scheme 1-5**). Thus, the increase of TA concentration promotes the formation of the $[\text{Ag}_2^+-\text{TA}]$ complex which slows down the conversion of Ag_2^+ into Ag_4^{2+} and leads to the slow particle formation, which in turn, favor the formation of large and polydisperse Ag NPs. On the contrary, at low concentrations, TA acts primary as a reducer leading the fast nucleation of monodisperse Ag NPs, following a conventional La Mer bust nucleation process (**Scheme 1-6**).

Based on this fact; we promote this initial fast reduction of Ag^+ ions by using low concentrations of TA leading to the formation of small, highly monodisperse Ag NPs.



Scheme 1- Reduction Mechanism of Silver Ions by TA. (1) Phenolic hydroxyls of TA undergo two-electron oxidation to the corresponding quinone form and donate two electrons for the reduction of Ag^+ precursor (2). At this moment, a two-step process takes place, the production of Ag^0 and the further formation of a new specie, Ag_2^+ (3). TA interacts with Ag_2^+ mediating its complexation (4). This $[\text{Ag}_2^+-\text{TA}]$ complex undergoes slower transformations compared to the uncomplexed Ag_2^+ , which leads to the formation of larger Ag NPs with irregular sizes (5, 6).

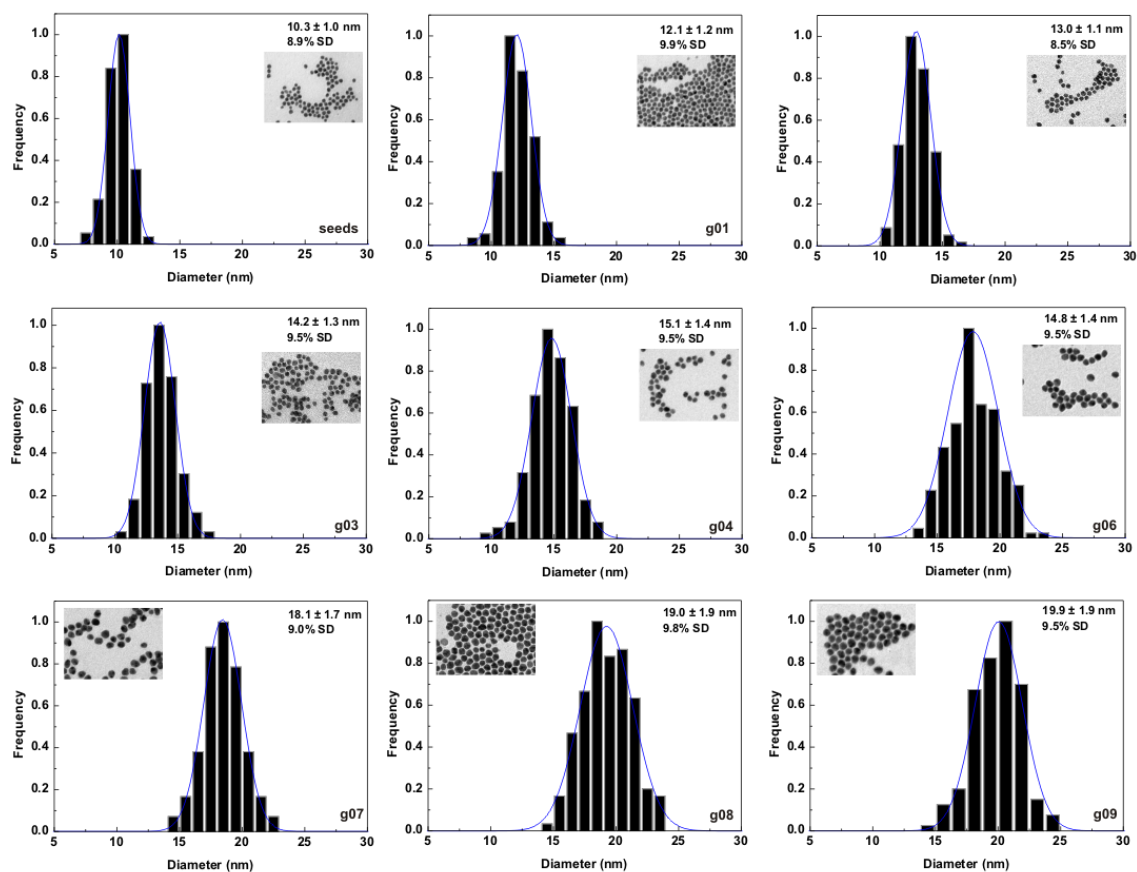


Figure S5- TEM image Analysis of Ag NPs shown in Figure 2. Ag seed diameter increases from 10.3 ± 10.9 nm to 19.9 ± 1.9 nm after different growing steps. In all cases, the concentration of the Au NP solution is the same ($\sim 6 \cdot 10^{12}$ NPs/mL). At least, 500 NPs were counted in each case.

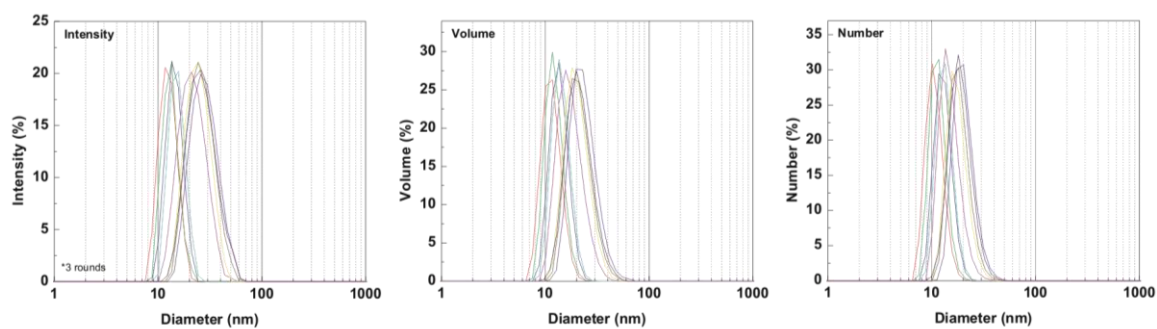


Figure S6- Size Distribution by Intensity (Left), Volume (Middle) and Number (Right) of silver colloids obtained after different growth steps.

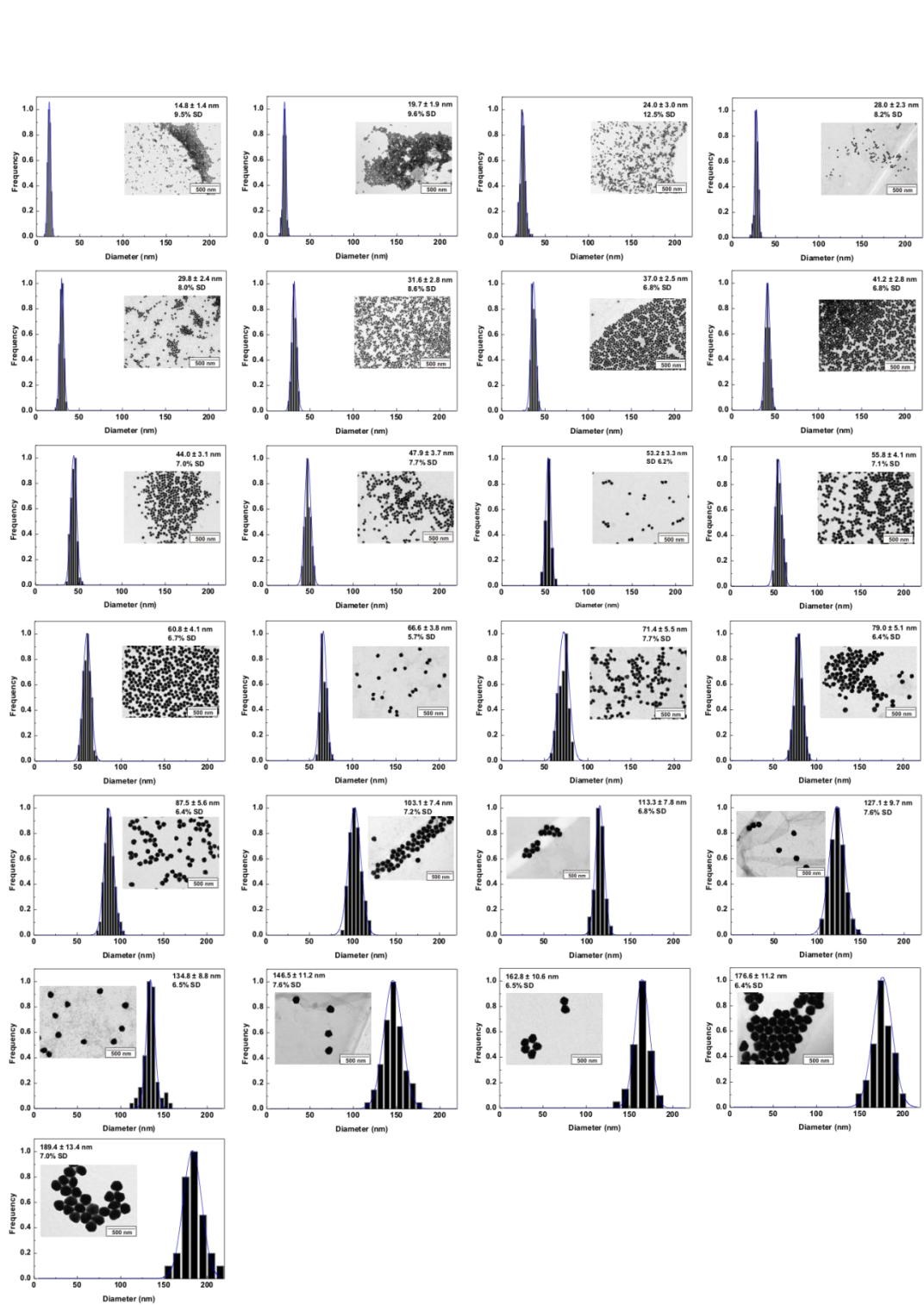


Figure S7- TEM image Analysis of Ag NPs shown in Figure 7. Ag seed diameter increases from 14.8 ± 1.4 nm to 189.4 ± 13.4 nm after different growing steps. At least, 500 NPs were counted in each case.

4. Calculated Spectra

Experimental absorbance was compared to calculations based on the standard Mie theory of spherical particles. Calculations of the scattering coefficient of colloidal Ag NPs of different diameters were obtained using Mie plot software considering Ag spheres embedded in water at 25 °C. Mean size and standard distribution measured by TEM were used for the calculations.

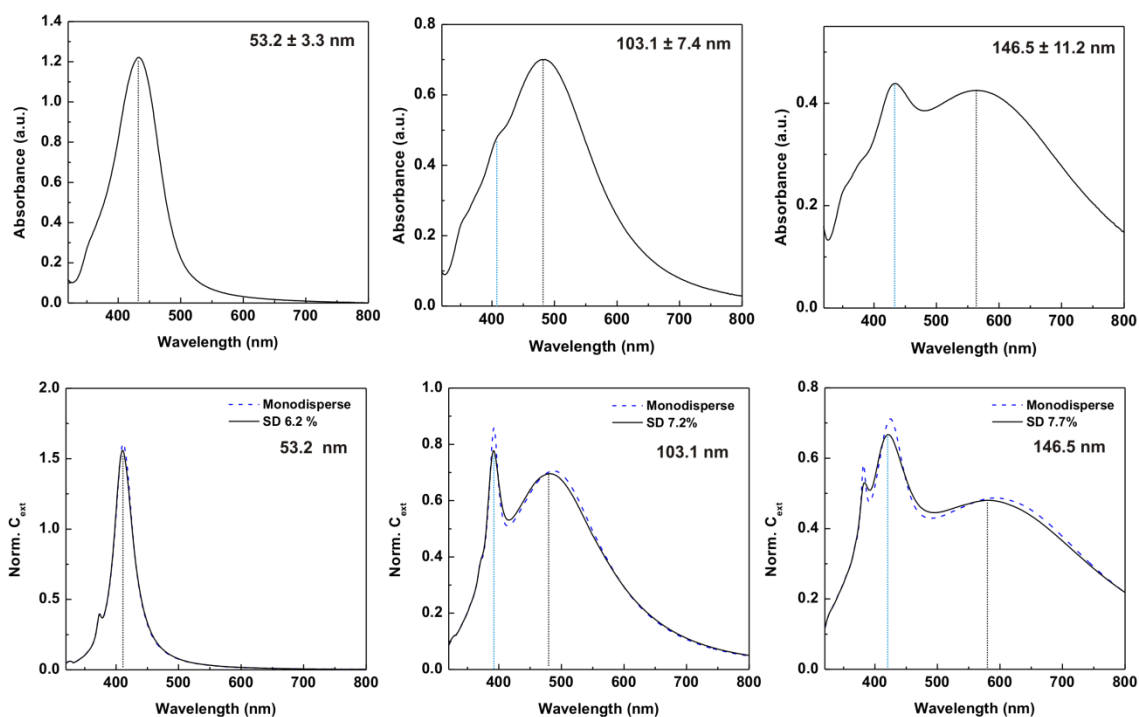


Figure S8. Top) Experimental absorption spectra of Ag NPs of different sizes 53.2 nm, 103.1 nm, and 146.5 nm. **Bottom)** Calculated extinction spectra of monodisperse Ag spheres (dashed line) and with the same mean size and size deviation as obtained experimentally (solid line).

5. Ligand Exchange of Ag Nanoparticles

Ligand exchange was performed by adding aqueous solution of known amounts of ligands (PVP or BSA) to as-synthesized Ag NPs solutions (final concentration 5 mM (PVP), 1mM BSA) under vigorous stirring. Functionalized Ag NPs were purified and further characterized by UV-Vis and DLS.

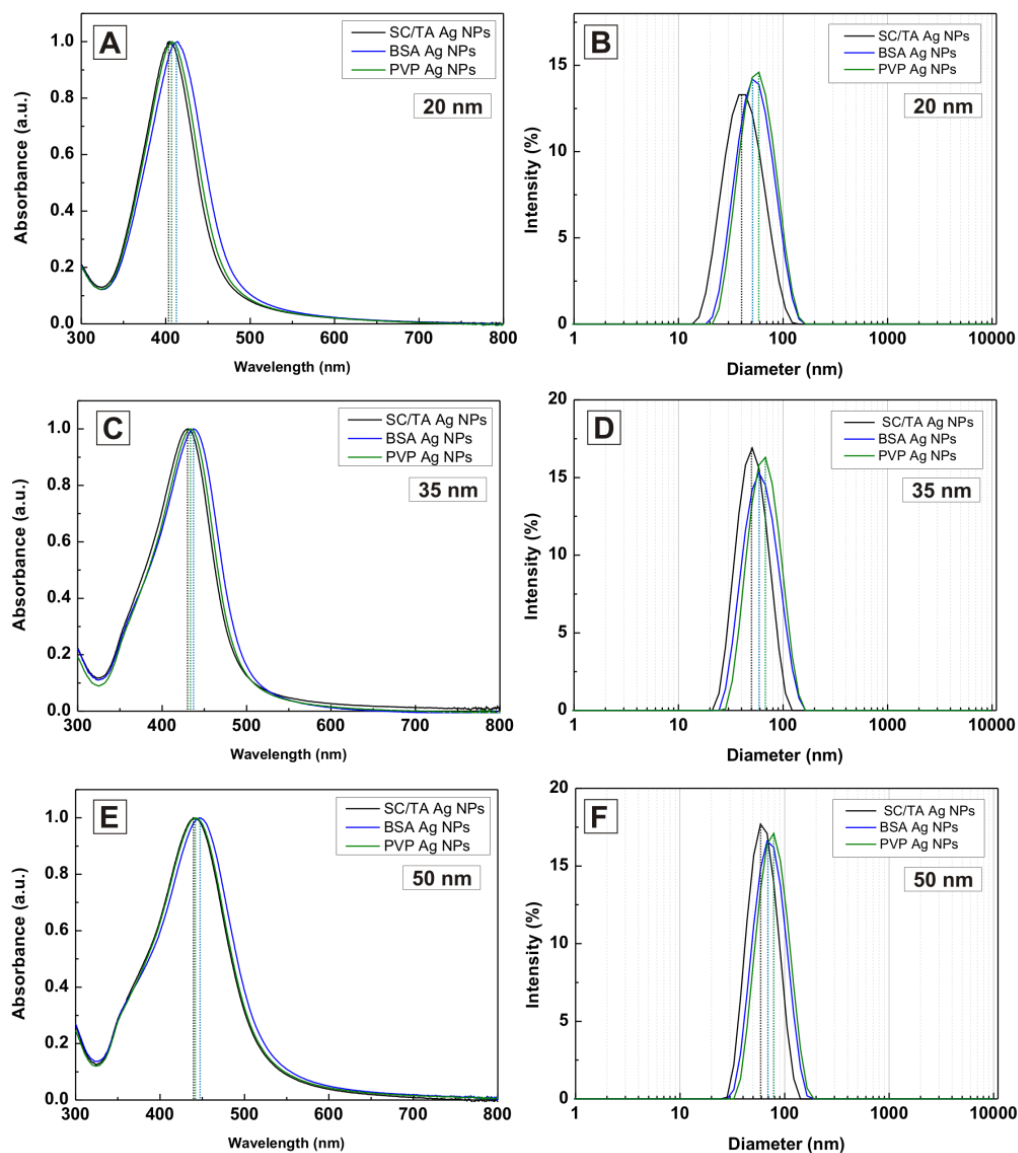


Figure S9. Functionalization of Ag NPs with PVP and BSA. UV-Vis spectra and DLS of Ag NPs of different sizes 20 nm (A, B), 35 nm (C, D) and 50 nm (E, F) recorded before (black line) and after the ligand exchange process with BSA (blue line) and PVP (green line). Once the native molecules are replaced by PVP or BSA the corresponding absorption peak shifts to the red and the hydrodynamic diameter increases.

References

- (1) Lee, P. C.; Meisel, D. *The Journal of Physical Chemistry* **1982**, *86*, 3391-3395.
- (2) Dadosh, T. *Materials Letters* **2009**, *63*, 2236-2238.
- (3) Rainville, L.; Dorais, M.-C.; Boudreau, D. *RSC Advances* **2013**, *3*, 13953-13960.
- (4) Slot, J. W.; Geuze, H. J. *European journal of cell biology* **1985**, *38*, 87-93.
- (5) Tao, A. R.; Habas, S.; Yang, P. *Small* **2008**, *4*, 310-325.
- (6) Bastús, N. G.; Comenge, J.; Puntès, V. c. *Langmuir* **2011**, *27*, 11098-11105.
- (7) Ji, X.; Song, X.; Li, J.; Bai, Y.; Yang, W.; Peng, X. *Journal of the American Chemical Society* **2007**, *129*, 13939-13948.
- (8) Janata, E.; Henglein, A.; Ershov, B. G. *The Journal of Physical Chemistry* **1994**, *98*, 10888-10890.
- (9) Pillai, Z. S.; Kamat, P. V. *The Journal of Physical Chemistry B* **2003**, *108*, 945-951.